Green Energy and Fuel Research

Scilight

Review

Carbon-Negative Characteristics of Biochar and Gas Emissions during Biomass Pyrolysis: A Mini Review

Che-Jung Hsu

Department of Marine Environmental Engineering, National Kaohsiung University of Science and Technology, Kaohsiung 811213, Taiwan; zachhsu@nkust.edu.tw; Tel.: +886-7-3617141 (ext. 23763)
Received: 29 May 2026; Revised: 29 August 2026; Accepted: 21 September 2026; Published: 29 September 2026

Abstract: Biomass pyrolysis has attracted increasing attention as a sustainable technology for simultaneous biochar production, renewable energy recovery, and carbon sequestration. This mini review discusses the carbon-negative characteristics of biochar, gas emissions during biomass pyrolysis, and the influence of pyrolysis conditions on syngas composition and carbon structural evolution. During pyrolysis, biomass undergoes devolatilization, deoxygenation, aromatization, and graphitization, producing gaseous products such as H_2, CO, CO_2, CH_4, and light hydrocarbons together with stable carbonaceous residues. Elevated pyrolysis temperatures generally enhance the formation of combustible gases, particularly H_2 and CO, while reducing oxygenated gases such as CO_2 due to intensified secondary cracking and deoxygenation reactions. Simultaneously, carbon structures progressively transform from disordered precursor molecules into aromatic and graphitic domains with improved physicochemical stability. Biomass species, reactor configuration, carrier gas atmosphere, and thermal conditions significantly affect gas evolution behavior and carbon conversion efficiency. Overall, biomass pyrolysis demonstrates strong potential for carbon-neutral energy production, greenhouse gas mitigation, and development of sustainable carbon materials within circular bioeconomy systems.

Keywords: biochar; pyrolysis; greenhouse gases; air pollution; carbon neutrality; carbon sequestration

1. Introduction

The increasing global demand for sustainable energy and carbon mitigation technologies has intensified interest in biomass pyrolysis and biochar production. Biomass residues generated from agriculture, forestry, and municipal activities represent abundant renewable resources that can be converted into valuable carbonaceous materials and energy products through thermochemical processes. Among these technologies, pyrolysis has attracted considerable attention because it simultaneously produces biochar, bio-oil, and combustible gaseous products under oxygen-limited conditions [1]. Biochar, a carbon-rich solid residue obtained from biomass carbonization, has been widely recognized for its potential applications in carbon sequestration [2], soil improvement [3], environmental remediation [4], and renewable energy systems [5]. Gui et al. (2025) reported that the input of biochar into soil adsorbs atmospheric carbon dioxide (CO_2) for carbon sequestration. Their prediction indicated that the biochar-cultivated top soils in China could reach 7.38–12.5 billion tons of carbon sequestration with an additional 0.34–2.66 billion tons of CO_2 capture [2]. Gaurav et al. (2025) reported that biochar provides abundant mineral nutrients and enhances their availability in soil [6]. By increasing soil electrical conductivity, it can facilitate the movement and delivery of essential elements, including Ca, Mg, and N, toward plant roots, thereby improving nutrient acquisition and supporting plant growth. Hsu et al. (2023) applied sulfurized magnetic biochar for active capping to remediate heavy metal contaminated sediment [4]. Their experimental result confirmed the effectiveness of sulfurized magnetic biochar in lowering aquatic Cu, Ni, Zn, Hg, and MeHg mobilities. Yang et al. (2024) mentioned that the addition Fe-containing biochar to food waste enhances thermophilic dark fermentation of hydrogen production [7]. Hydrogen production increased by approximately 31.19% by Fe-containing biochar addition.

Biochar has gained particular scientific and industrial interest because of its carbon-negative characteristics. During photosynthesis, plants capture atmospheric CO_2 and store carbon within biomass. Through pyrolysis, a significant fraction of this carbon is transformed into highly aromatic and recalcitrant structures that are resistant to biological degradation, thereby enabling long-term carbon storage in soils and environmental matrices [8].

Furthermore, biochar production can reduce greenhouse gas emissions by displacing fossil fuel consumption through recovery of syngas and thermal energy generated during pyrolysis. Consequently, biomass pyrolysis has been regarded as a promising strategy for climate change mitigation and circular bioeconomy development.

In addition to biochar formation, gaseous emissions generated during pyrolysis play critical roles in determining process efficiency, energy recovery, and environmental impacts. Pyrolysis gases commonly contain hydrogen (H_2), carbon monoxide (CO), CO_2, methane (CH_4), and various light hydrocarbons (HCs), with their composition strongly influenced by biomass type, reactor configuration, heating rate, residence time, and pyrolysis temperature [9]. Numerous studies have demonstrated that elevated pyrolysis temperatures promote secondary cracking and deoxygenation reactions, thereby enhancing production of combustible gases such as H_2 and CO while reducing oxygenated species such as CO_2 [10]. Simultaneously, thermal treatment progressively transforms disordered biomass structures into increasingly aromatic and graphitic carbon materials through dehydration, aromatization, and graphitization reactions.

Therefore, understanding gas evolution behavior and carbon structural transformation during biomass pyrolysis is essential for optimizing biochar production, improving syngas quality, and maximizing carbon sequestration efficiency. This mini review discusses the carbon-negative characteristics of biochar, gas emissions during pyrolysis, carbon conversion mechanisms, and the influence of biomass species and pyrolysis parameters on syngas composition and carbon structure evolution.

2. Literature Search Strategy of This Mini Review

A literature search was conducted using Web of Science, Scopus, and Google Scholar to identify relevant peer-reviewed studies. The search employed combinations of the keywords “biochar”, “biomass pyrolysis”, “carbon sequestration”, “carbon negative”, “syngas”, “gas emissions”, “pyrolysis temperature”, “hydrogen production”, “carbon structure”, “graphitization”, “life-cycle assessment”, and “techno-economic analysis”. Studies published primarily between 2015 and 2026 were considered to capture recent developments, while earlier seminal studies were included where necessary to establish fundamental concepts and mechanisms. Studies were selected based on their relevance to biochar carbon negativity, pyrolysis-induced gas evolution, syngas composition, carbon structural transformation, and the environmental and economic feasibility of biochar production.

3. Biochar and Its Carbon Negativity

Figure 1 compares the natural carbon cycle in vegetation and soil with the biochar carbon cycle, illustrating why biochar is widely regarded as a carbon-negative material and a promising negative-emission technology. In the conventional terrestrial carbon cycle, atmospheric carbon dioxide (CO_2) is assimilated by plants through photosynthesis and incorporated into living biomass. After plant senescence, the biomass undergoes microbial decomposition and mineralization in soil, eventually releasing most of the captured carbon back into the atmosphere as CO_2 through respiration. Consequently, although vegetation temporarily stores atmospheric carbon, the majority of this carbon is recycled within relatively short ecological timescales.

The right side of Figure 1 demonstrates how pyrolysis fundamentally alters this carbon cycle. During pyrolysis, biomass is thermochemically converted under oxygen-limited conditions, producing biochar, syngas, bio-oil, and thermal energy. Approximately half of the biomass carbon may be released as gases or utilized for energy generation, while a substantial fraction is transformed into highly aromatic and recalcitrant carbon structures that constitute biochar. Because this carbon is chemically stable and resistant to microbial degradation, it can persist in soils for centuries to millennia, thereby functioning as a long-term carbon sink. This process effectively removes atmospheric CO_2 from the active carbon cycle and stores it in a semi-permanent form [11,12].

The carbon-negative characteristic of biochar arises from several complementary mechanisms. First, plants initially capture atmospheric CO_2 through photosynthesis, converting inorganic carbon into biomass carbon. Rather than allowing this biomass to naturally decompose and rapidly return CO_2 to the atmosphere, pyrolysis stabilizes a large portion of the carbon into condensed aromatic structures. These structures contain polyaromatic and graphitic domains that are highly resistant to biological and chemical oxidation. Lehmann and Joseph’s foundational biochar research demonstrated that pyrolysis significantly slows carbon mineralization rates compared with uncharred organic matter, enabling long-term carbon sequestration [13]. Studies have shown that biochar decomposition rates may be one or two orders of magnitude slower than those of fresh biomass [14–16]. Table 1 highlights substantial differences in the global warming potential (GWP) associated with the production of representative porous adsorbent materials. Biochar exhibits the lowest environmental burden, with GWP values ranging from −1.1 to 13.70 kg CO_2-eq/kg. Negative values indicate that carbon sequestration can offset greenhouse gas emissions generated during biomass conversion. Activated carbon shows a positive but highly variable GWP

(0.8752–47.15 kg CO_2-eq/kg), reflecting differences in feedstocks, activation processes, and energy requirements. In contrast, zeolites and graphene oxide exhibit substantially higher GWP values, reaching 1733.3 and 4841 kg CO_2-eq/kg, respectively, primarily indicating energy- and resource-intensive synthesis. MOFs display the widest range (0.0613–1136.2 kg CO_2-eq/kg), demonstrating strong dependence on synthesis routes and precursors. COFs show moderate positive GWP values of 48.9–61.5 kg CO_2-eq/kg. Overall, biochar offers considerable potential as a comparatively low-carbon porous material for sustainable environmental applications.

Table 1. Comparison of GWP and associated environmental impact classifications for developed materials.

Material	GWP (kg CO_2-eq/kg)	Classification	Reference
Biochar	−1.1–13.70	Negative/positive	[17–19]
Activated carbon	0.8752–47.15	Positive	[20–24]
Zeolite	833.3–1733.3	Positive	[25]
Graphene oxide	1186–4841	Positive	[26]
MOF	0.0613–1136.2	Positive	[27–29]
COF	48.9–61.5	Positive	[30]

Second, the pyrolysis process itself can offset fossil fuel consumption. As illustrated in the Figure 1, approximately 50% of the biomass energy content can be recovered as heat, electricity, transportation fuels, or co-products. When bioenergy generated during pyrolysis replaces fossil-based energy sources, additional greenhouse gas emissions are avoided. Therefore, biochar systems provide dual climate benefits: stable carbon sequestration and displacement of fossil fuel emissions. Woolf et al. estimated that sustainable global biochar implementation could mitigate up to 1.8 billion tonnes of CO_2-equivalent emissions annually through combined sequestration and emission-offset effects [8].

Third, biochar amendments can indirectly enhance soil carbon storage and reduce greenhouse gas emissions from soils. Biochar possesses high surface area, microporosity, and aromaticity, which influence microbial activity and soil organic matter dynamics. Numerous studies have reported that biochar can induce "negative priming effects", wherein microbial decomposition of native soil organic carbon decreases following biochar addition [11,31]. This suppression of soil carbon mineralization reduces CO_2 emissions from soil respiration and enhances long-term soil carbon accumulation. Furthermore, biochar improves soil aggregation, water retention, cation exchange capacity, and microbial habitat quality, thereby promoting biomass productivity and additional atmospheric carbon fixation through enhanced plant growth [32,33].

Figure 1 also highlights the importance of pyrolysis conditions in determining carbon sequestration efficiency. Higher pyrolysis temperatures generally increase aromatic condensation and carbon stability, producing biochars with greater resistance to degradation. Biochars generated above approximately 500 °C often exhibit higher fixed carbon content and lower volatile fractions, making them particularly suitable for long-term sequestration [34]. However, the long-term carbon sequestration potential of biochar remains uncertain because its persistence depends on feedstock properties, pyrolysis conditions, and post-application environmental conditions. Although aromatic carbon may persist for centuries, it can undergo gradual oxidation and microbial decomposition. Moreover, higher pyrolysis temperatures improve carbon stability but reduce biochar yield, creating a trade-off between carbon persistence and total carbon retained. Therefore, the optimization of feedstock type and pyrolysis conditions, and the selection of the application field are essential for maximizing carbon-negative performance.

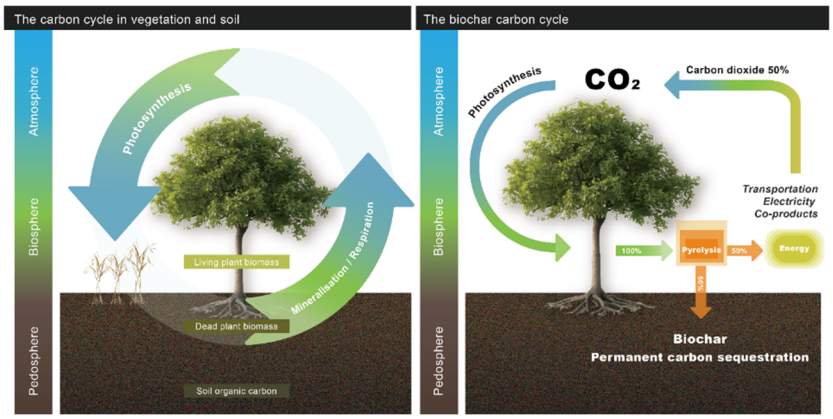

Figure 1. The carbon cycle versus the biochar carbon cycle (concepts described by Woolf et al. [8] and Steiner [35]).

Figure 2 illustrates the progressive physicochemical transformation of biomass-derived carbon during pyrolysis and high-temperature carbonization, emphasizing the relationship between gas emissions, carbon structure evolution, and graphitization. Biomass pyrolysis is a thermochemical conversion process conducted in oxygen-limited or oxygen-free conditions, during which complex organic macromolecules decompose into gaseous products, condensable vapors, and solid carbonaceous residues. Figure 2 also illustrates how increasing temperature promotes volatilization, aromatization, dehydrogenation, and structural ordering of carbon materials from precursor molecules to graphitic carbon.

At room temperature, biomass consists primarily of cellulose, hemicellulose, lignin, proteins, lipids, and extractives containing abundant oxygenated and hydrogenated functional groups [9]. These precursor molecules possess highly disordered structures with mixed aliphatic and aromatic components. Upon heating, thermal decomposition begins through cleavage of weak chemical bonds such as C–O, C–H, and C–C linkages. Pyrolysis generally occurs between approximately 300 and 700 °C, although decomposition behavior depends strongly on biomass composition and heating conditions. The figure indicates that gaseous emissions peak around 300–350 °C, which corresponds closely with the major devolatilization stage reported in thermogravimetric and pyrolysis studies. Hemicellulose typically decomposes between 200–300 °C, cellulose between 300–400 °C, and lignin over a broader range extending beyond 500 °C [10].

During this active pyrolysis stage, large quantities of gaseous species, including CO_2, H_2, CO, CH_4, and other hydrocarbons are released, as illustrated in the Figure 2 [36,37]. CO_2 and CO are primarily generated through decarboxylation and decarbonylation reactions involving oxygen-containing functional groups. Hydrogen evolution mainly originates from dehydrogenation and cracking reactions, while hydrocarbon gases result from fragmentation of aliphatic chains and tar compounds. Studies have shown that increasing pyrolysis temperature generally enhances secondary cracking reactions, thereby increasing H_2 and CO yields while decreasing condensable tar fractions. The release of volatile matter simultaneously creates pores and defects within the residual char structure. As temperature approaches approximately 700 °C, the carbonaceous residue evolves into amorphous carbon containing both sp^2 and sp^3 hybridized carbon domains, as shown in the figure [38]. At this stage, dehydration and condensation reactions promote the formation of small aromatic clusters [38,39]. However, the structure remains highly disordered, containing randomly oriented graphene-like fragments interconnected with residual aliphatic structures. Considerable heteroatom content and structural defects are still present. According to carbonization theory, this stage represents incomplete aromatization and limited crystallographic ordering.

Further heating to approximately 1200 °C promotes the formation of predominantly sp^2-hybridized amorphous carbon by facilitating the rearrangement and fusion of aromatic clusters into larger conjugated structures [38,39]. The continued elimination of hydrogen and oxygen through secondary devolatilization significantly increases the fixed carbon content and aromaticity of the material. Raman spectroscopy and X-ray diffraction studies consistently demonstrate increasing graphitic ordering and decreasing structural disorder with elevated pyrolysis temperature [38]. Simultaneously, hydrogen generation often increases because dehydrogenation reactions become thermodynamically favorable at higher temperatures.

The figure subsequently depicts the transition from non-graphitic carbon to graphitic carbon between approximately 1400 and 1700 °C [38]. Non-graphitic carbon, often referred to as turbostratic carbon, consists of misaligned graphene-like layers with limited crystallite growth. Structural defects, cross-linking, and non-hexagonal carbon rings hinder perfect graphitic ordering. As temperature further increases, carbon atoms gain sufficient mobility to reorganize into more ordered hexagonal graphene layers. This graphitization process reduces defects, enlarges aromatic lamellae, and improves crystallinity. Franklin's classical theory distinguished graphitizing and non-graphitizing carbons based on their ability to develop ordered graphite structures upon high-temperature treatment.

Recent studies have further demonstrated that catalytic pyrolysis can significantly accelerate graphitization while simultaneously enhancing hydrogen production [40,41]. Metal catalysts such as Fe, Co, and Ni facilitate carbon atom diffusion and aromatic layer rearrangement, lowering the graphitization temperature and promoting the formation of porous graphitic carbon. Fe–Co catalysts, for example, have been shown to improve both hydrogen yield and graphitic ordering during biomass pyrolysis.

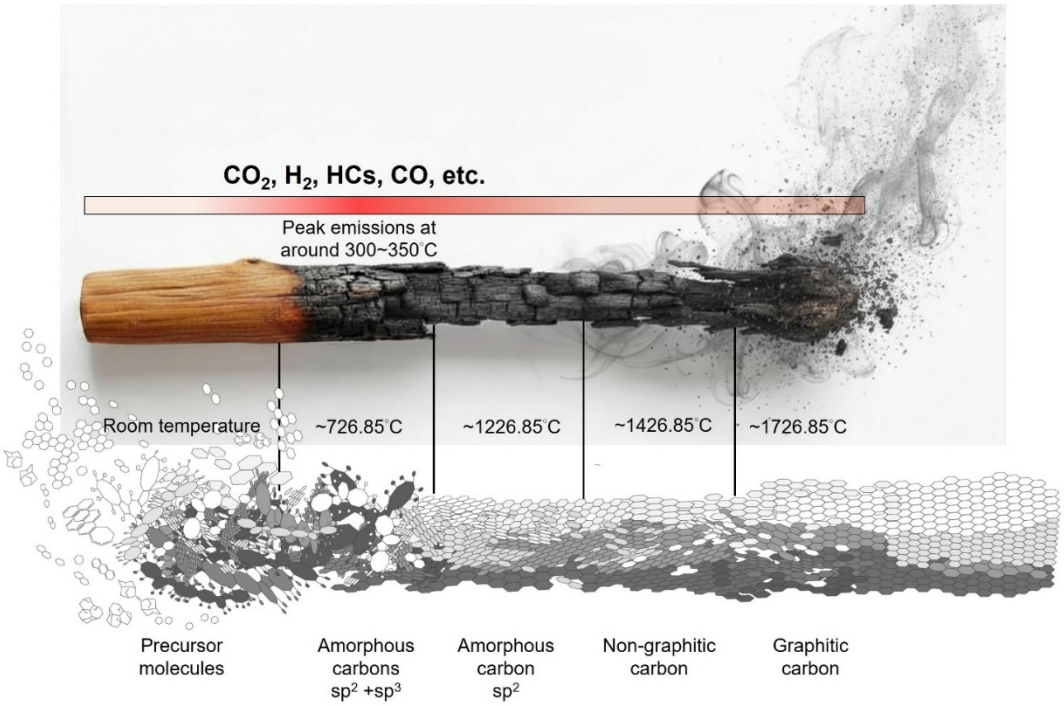

Figure 2. Gas emissions and carbon conversion during biomass pyrolysis.

4. Plant Types, Species, and Pyrolysis Parameters

Table 2 compares the composition of gaseous products generated during biomass pyrolysis under different temperatures, feedstocks, and reactor conditions. The data demonstrate that pyrolysis temperature and biomass composition strongly influence the distribution of syngas components, particularly HCs, CO, CO_2, and H_2. Overall, increasing pyrolysis temperature generally enhances the formation of combustible gases such as H_2 and CO, while reducing oxygenated gases such as CO_2, indicating progressive carbonization and secondary cracking reactions at elevated temperatures.

Among the investigated feedstocks, pine sawdust exhibited significant variation in gas composition with increasing temperature from 600 to 900 °C. At 600 °C, the gaseous products contained approximately 14.82% HCs, 46.68% CO, 24.87% CO_2, and 10.45% H_2 [42]. As the temperature increased to 800 °C, HC content slightly decreased while CO concentration increased substantially to 40.13%, accompanied by elevated H_2 production. This trend suggests that secondary thermal cracking and deoxygenation reactions became dominant at higher temperatures, promoting conversion of condensable volatiles into permanent gases [43,44]. Simultaneously, the decline in CO_2 concentration indicates progressive removal of oxygen-containing functional groups during carbonization.

Eastern redcedar (*Juniperus virginiana*) displayed similar thermal behavior [45]. At 350 °C, the gas stream was dominated by CO_2 (47.44%), indicating that decarboxylation reactions were the primary decomposition pathway during low-temperature pyrolysis [46–48]. However, increasing the temperature to 500 °C resulted in markedly higher CO production (49.06%) and increased H_2 generation. The elevated CO yield is associated with enhanced decarbonylation and cleavage of lignocellulosic structures [49,50]. These results further demonstrate that intermediate pyrolysis temperatures favor the production of combustible syngas components.

The grape-derived biomass showed a particularly strong temperature dependence [51]. At 400 °C, CO_2 represented approximately 80.53% of the gaseous products, whereas H_2 content remained very low. As the temperature increased to 700 °C, H_2 concentration rose dramatically to 28.80%, while CO_2 decreased to 20.62%. The substantial increase in hydrogen generation at elevated temperatures is attributable to intensified dehydrogenation, aromatization, and reforming reactions. The simultaneous increase in CO concentration also reflects enhanced cracking of tar intermediates and oxygenated compounds.

Rice husk pyrolysis exhibited comparable trends [51]. At 400 °C, CO_2 remained the dominant gaseous product, accounting for more than 80% of total gases. However, increasing temperature progressively enhanced CO and H_2 production while suppressing CO_2 formation. At 700 °C, H_2 concentration reached 19.20%, indicating significant thermal conversion of biomass-derived volatiles into syngas. The high silica content of rice husk may also influence catalytic cracking reactions and gas evolution behavior during pyrolysis [52,53].

Coconut shell and bamboo demonstrated similar thermal decomposition characteristics [54,55]. For coconut shell, increasing temperature from 400 to 700 °C elevated H_2 concentration from 2.10% to 5.70% and increased

CO generation, while CO_2 declined substantially. Bamboo pyrolysis also showed enhanced syngas quality at higher temperatures, with H_2 concentration increasing from 8.10% at 400 °C to 19.80% at 700 °C. The increase in H_2 and CO across both feedstocks suggests intensified secondary devolatilization and aromatic condensation reactions during high-temperature pyrolysis [56].

Overall, the table clearly demonstrates that pyrolysis temperature is one of the most influential parameters governing syngas composition. Lower temperatures favor CO_2-rich gas streams dominated by primary devolatilization reactions, whereas higher temperatures promote formation of H_2- and CO-rich syngas through cracking, reforming, and deoxygenation mechanisms. Biomass composition, reactor configuration, heating rate, and carrier gas conditions further contribute to variations in gas yield and composition. These findings highlight the importance of optimizing pyrolysis parameters to maximize syngas quality and improve the efficiency of biomass-to-energy conversion systems.

Table 2. Comparison of syngas composition and pyrolysis parameters.

Biomass	Temperature (°C)	Types of Gaseous Substances Percentage (%)				Furnace or Reactor	Reference
		HCs	CO	CO_2	H_2		
Pine sawdust	600	14.82	46.68	24.87	10.45	Tubular furnace 0.05 L/min N_2	[42]
	700	13.89	47.19	20.76	13.89		
	800	16.75	46.12	16.02	17.78		
	900	14.65	45.74	10.06	25.59		
Eastern redcedar wood	450	14.51	37.27	44.56	3.01	Parr reactor at 6 °C/min under N_2.	[45]
	500	16.41	40.42	40.03	3.14		
Grape	400	4.00	29.00	66.20	0.80	Tubular furnace 0.25 L/min N_2	[51]
	500	12.00	23.20	58.00	6.80		
	600	16.60	20.00	43.00	20.60		
	700	18.60	20.40	31.60	29.20		
	800	19.20	29.60	22.40	28.80		
Rice husk	400	3.00	40.80	53.60	1.20	Tubular furnace 0.25 L/min N_2	[51]
	500	7.40	40.80	35.40	4.20		
	600	7.60	48.60	24.60	10.80		
	700	6.20	50.40	18.80	18.60		
	800	11.80	43.80	18.00	19.20		
Coconut shell	400	7.10	31.70	33.28	2.10	Fixed-bed pyrolysis at 10 °C/min under Ar	[55]
	500	7.25	32.63	34.48	2.90		
	600	7.35	33.43	26.60	3.70		
	700	7.42	34.26	35.05	4.50		
	800	7.40	35.76	34.05	5.70		
Bamboo	300	1.60	27.30	66.70	2.90	Pyrolysis furnace at 10 °C/min under N_2.	[54]
	400	6.40	36.30	47.90	8.10		
	500	11.80	36.40	41.30	9.20		
	600	12.30	33.50	37.90	14.20		
	700	13.70	31.80	33.40	19.80		

5. Commercial Viability of Biochar Production

For the techno-economic analysis (TEA), annualized capital expenditure (CAPEX), operating expenditure (OPEX), and the costs of feedstock handling and energy consumption are generally used to evaluate the commercial viability of biochar production and application [57,58]. Tang et al. (2026) reported that annualized CAPEX was the primary economic burden of the biochar production system. Of this expenditure, the pyrolysis unit represented 63%, followed by dewatering facilities (32%) and drying equipment (5%). OPEX was another substantial component, with labour costs comprising more than 90% of this category [58]. Biomass pyrolysis also incurred substantial material and energy expenses, with electricity responsible for approximately 99% of these costs. Expenditures associated with other processing stages were comparatively insignificant. Across the entire biochar production system, electricity accounted for nearly 30% of total expenditure, emphasizing energy consumption as an important factor influencing overall production economics.

6. Conclusions, Challenges, and Future Perspectives

Biomass pyrolysis represents a promising thermochemical pathway for simultaneous biochar production, renewable energy recovery, and greenhouse gas mitigation. This mini review highlights the carbon-negative characteristics of biochar and the critical relationship between pyrolysis conditions, gas emissions, and carbon structural evolution. During pyrolysis, biomass undergoes progressive devolatilization, deoxygenation, aromatization, and graphitization, resulting in the formation of syngas and increasingly stable carbonaceous materials. Elevated pyrolysis temperatures generally enhance the production of combustible gases such as H_2 and CO while reducing CO_2 emissions, indicating intensified secondary cracking and carbonization reactions. In

parallel, carbon structures gradually evolve from disordered precursor molecules into aromatic and graphitic domains with improved physicochemical stability.

The reviewed studies further demonstrate that biomass type, reactor configuration, carrier gas atmosphere, and heating conditions significantly influence syngas composition and carbon conversion efficiency. Feedstocks such as pine sawdust, grape residues, rice husk, coconut shell, and bamboo exhibit distinct gas evolution behaviors due to differences in lignocellulosic composition and mineral content. Optimization of pyrolysis parameters is therefore essential to maximize hydrogen-rich syngas generation, improve biochar quality, and enhance long-term carbon sequestration potential.

Present knowledge of biomass pyrolysis remains limited by the complex interactions among feedstock composition, reactor configuration, carrier gas atmosphere, and thermal conditions, which hinder consistent prediction of syngas composition and carbon conversion efficiency. The trade-off between biochar yield, carbon stability, and energy recovery also remains insufficiently resolved.

Future research should focus on developing catalytic and energy-efficient pyrolysis systems capable of simultaneously enhancing syngas quality and graphitic carbon formation. Advanced catalysts, particularly transition metal-based systems, may further reduce graphitization temperature and improve hydrogen production efficiency. In addition, more comprehensive life-cycle assessments and techno-economic analyses are still required to evaluate the large-scale feasibility and environmental sustainability of biomass pyrolysis technologies. Further investigation into the long-term environmental behavior, stability, environmental impacts, and functional applications of biochar will also be essential for advancing its implementation in carbon neutrality strategies, sustainable agriculture, and circular bioeconomy systems.

Funding: This study was supported by the Marine Sustainable Development and Research Project of the National Kaohsiung University of Science and Technology (NKUST) under the 2025 Higher Education SPROUT Project of the Ministry of Education of Taiwan (ROC) and the National Science and Technology Council (NSTC 113-2628-E-992-001-MY3).

Institutional Review Board Statement: Not applicable.

Informed Consent Statement: Not applicable.

Data Availability Statement: Data will be made applicable on request.

Conflicts of Interest: The author declares no conflict of interest.

Use of AI and AI-Assisted Technologies: During the preparation of this work, the author used ChatGPT (OpenAI) to improve the quality of the diagrams. After using this tool, the author reviewed and edited the content as needed and takes full responsibility for the content of the published article.

References

1. Antal, M.J.; Grønli, M. The art, science, and technology of charcoal production. *Ind. Eng. Chem. Res.* **2003**, *42*, 1619–1640. https://doi.org/10.1021/ie0207919.
2. Gui, X.; Xu, X.; Zhang, Z.; et al. Biochar-amended soil can further sorb atmospheric CO_2 for more carbon sequestration. *Commun. Earth Environ.* **2025**, *6*, 5. https://doi.org/10.1038/s43247-024-01985-5.
3. Shyam, S.; Ahmed, S.; Joshi, S.J.; et al. Biochar as a Soil amendment: Implications for soil health, carbon sequestration, and climate resilience. *Discov. Soil* **2025**, *2*, 18. https://doi.org/10.1007/s44378-025-00041-8.
4. Hsu, C.J.; Cheng, Y.H.; Chung, A.; et al. Using recoverable sulfurized magnetic biochar for active capping to remediate multiple heavy metal contaminated sediment. *Environ. Pollut.* **2023**, *316*, 120555. https://doi.org/10.1016/j.envpol.2022.120555.
5. Yan, K.; Yang, X.; Yuan, Q. Biochar for carbon-negative hydrogen production from fossil fuel reservoirs. *J. Clean. Prod.* **2025**, *505*, 145463. https://doi.org/10.1016/j.jclepro.2025.145463.
6. Gaurav, S.; Diptanu, B.; Mehta, C.M.; et al. Effects of biochar amendment at various soil depths on maize roots and growth indices. *Sci. Rep.* **2025**, *15*, 26310. https://doi.org/10.1038/s41598-025-09218-1.
7. Yang, Y.; Bu, J.; Tiong, Y.W.; et al. Enhanced thermophilic dark fermentation of hydrogen production from food waste by Fe-modified biochar. *Environ. Res.* **2024**, *244*, 117946. https://doi.org/10.1016/j.envres.2023.117946.
8. Woolf, D.; Amonette, J.E.; Street-Perrott, F.A.; et al. Sustainable biochar to mitigate global climate change. *Nat. Commun.* **2010**, *1*, 56. https://doi.org/10.1038/ncomms1053.
9. Shen, Y.; Ma, D.; Ge, X. CO_2-looping in biomass pyrolysis or gasification. *Sustain. Energy Fuels* **2017**, *1*, 1700–1729. https://doi.org/10.1039/c7se00279c.
10. Devi, M.; Rawat, S.; Sharma, S. A comprehensive review of the pyrolysis process: From carbon nanomaterial synthesis to waste treatment. *Oxf. Open Mater. Sci.* **2021**, *1*, itab014. https://doi.org/10.1093/oxfmat/itab014.

11. Biswal, B.K.; Balasubramanian, R. Use of biomass-derived biochar as a sustainable material for carbon sequestration in soil: Recent advancements and future perspectives. *Npj Mater. Sustain.* **2025**, *3*, 26. https://doi.org/10.1038/s44296-025-00066-8.
12. Zhang, S.; Wang, S.; Zhang, J.; et al. Research on the application of biochar in carbon sequestration: A bibliometric analysis. *Energies* **2025**, *18*, 2745. https://doi.org/10.3390/en18112745.
13. Lehmann, J.; Joseph, S. *Biochar for Environmental Management: Science, Technology and Implementation*, 3nd ed. Routledge, Oxfordshire, UK, 2015.
14. Joseph, S.; Cowie, A.L.; Van Zwieten, L.; et al. How biochar works, and when it doesn't: A review of mechanisms controlling soil and plant responses to biochar. *GCB Bioenergy* **2021**, *13*, 1731–1764. https://doi.org/10.1111/gcbb.12885.
15. Li, H.; Azzi, E.S.; Sundberg, C.; et al. Can inert pool models improve predictions of biochar long-term persistence in soils? *Geoderma* **2024**, *452*, 117093. https://doi.org/10.1016/j.geoderma.2024.117093.
16. Ntonta, S.; Mathew, I.; Zengeni, R.; et al. Crop residues differ in their decomposition dynamics: Review of available data from world literature. *Geoderma* **2022**, *419*, 115855. https://doi.org/10.1016/j.geoderma.2022.115855.
17. Divyangkumar, N.; Panwar, N.L.; Agrawal, C.; et al. Cradle-to-gate analyses of biochar produced from agricultural crop residues by vacuum pyrolysis. *Clean Energy* **2024**, *8*, 1–15. https://doi.org/10.1093/ce/zkae069.
18. Kavindi, G.A.G.; Tang, L.; Sasaki, Y. Assessing GHG Emission Reduction in Biomass-Derived Biochar Production via Slow Pyrolysis: A Cradle-to-gate LCA Approach. *Resour. Conserv. Recycl.* **2025**, *212*, 107900. https://doi.org/10.1016/j.resconrec.2024.107900.
19. Raj, R.S.; Jain, S.; Sharma, A.K.; et al. Biochar production from rice husk: A comparative life cycle assessment of grid, biomass, and solar-powered pyrolysis. *Energies* **2026**, *19*, 1344. https://doi.org/10.3390/en19051344.
20. Arena, N.; Lee, J.; Clift, R. Life Cycle Assessment of activated carbon production from coconut shells. *J. Clean. Prod.* **2016**, *125*, 68–77. https://doi.org/10.1016/j.jclepro.2016.03.073.
21. Hjaila, K.; Baccar, R.; Sarrà, M.; et al. Environmental impact associated with activated carbon preparation from olive-waste cake via life cycle assessment. *J. Environ. Manag.* **2013**, *130*, 242–247. https://doi.org/10.1016/j.jenvman.2013.08.061.
22. Liao, M.; Kelley, S.; Yao, Y. Generating energy and greenhouse gas inventory data of activated carbon production using machine learning and kinetic based process simulation. *ACS Sustain. Chem. Eng.* **2019**, *8*, 1252–1261. https://doi.org/10.1021/acssuschemeng.9b06522.
23. Saleem, J.; Khalid Baig Moghal, Z.; Tahir, F.; et al. Life cycle assessment of high value activated carbon production based on mass and functional performance metrics. *Sci. Rep.* **2025**, *15*, 32797. https://doi.org/10.1038/s41598-025-16300-1.
24. Sepúlveda-Cervantes, C.V.; Soto-Regalado, E.; Rivas-García, P.; et al. Technical-environmental optimisation of the activated carbon production of an agroindustrial waste by means response surface and life cycle assessment. *Waste Manag. Res. J. a Sustain. Circ. Econ.* **2018**, *36*, 121–130. https://doi.org/10.1177/0734242x17741680.
25. Tobarameekul, P.; Worathanakul, P. Heat management options to reduce carbon footprint of green zeolite faujasite synthesis from rice husk ash. *Thai Environ. Eng. J.* **2021**, *35*, 59–68.
26. Bahmei, F.; Bahramifar, N.; Ghasemi, S.; et al. Comparison of environmental impacts in the production of graphene from biomass waste and the Hummers' method. *J. Clean. Prod.* **2025**, *497*, 145145. https://doi.org/10.1016/j.jclepro.2025.145145.
27. Escobar-Hernandez, H.U.; Quan, Y.; Papadaki, M.I.; et al. Life cycle assessment of metal–organic frameworks: Sustainability study of zeolitic imidazolate framework-67. *ACS Sustain. Chem. Eng.* **2023**, *11*, 4219–4225. https://doi.org/10.1021/acssuschemeng.2c07276.
28. Grande, C.A.; Blom, R.; Spjelkavik, A.; et al. Life-cycle assessment as a tool for eco-design of metal-organic frameworks (MOFs). *Sustain. Mater. Technol.* **2017**, *14*, 11–18. https://doi.org/10.1016/j.susmat.2017.10.002.
29. Luo, H.; Cheng, F.; Huelsenbeck, L.; et al. Comparison between conventional solvothermal and aqueous solution-based production of UiO-66-NH2: Life cycle assessment, techno-economic assessment, and implications for CO_2 capture and storage. *J. Environ. Chem. Eng.* **2021**, *9*, 105159. https://doi.org/10.1016/j.jece.2021.105159.
30. Espada, J.J.; Rodríguez, R.; de la Peña, A.; et al. Environmental impact analysis of surface printing and 3D inkjet printing applications using an imine based covalent organic framework: A life cycle assessment study. *J. Clean. Prod.* **2023**, *395*, 136381. https://doi.org/10.1016/j.jclepro.2023.136381.
31. Enebe, M.C.; Ray, R.L.; Griffin, R.W. The impacts of biochar on carbon sequestration, soil processes, and microbial communities: A review. *Biochar* **2025**, *7*, 107. https://doi.org/10.1007/s42773-025-00499-3.
32. Islam, M.U.; Jiang, F.; Guo, Z.; et al. Does biochar application improve soil aggregation? A meta-analysis. *Soil Tillage Res.* **2021**, *209*, 104926. https://doi.org/10.1016/j.still.2020.104926.
33. Sun, F.; Lu, S. Biochars improve aggregate stability, water retention, and pore-space properties of clayey soil. *J. Plant Nutr. Soil Sci.* **2014**, *177*, 26–33. https://doi.org/10.1002/jpln.201200639.

34. Lv, P.; Huan, Q.; Song, M. A review of biochar toward carbon neutrality: Production optimization and carbon sequestration potential assessment. *Carbon Neutral Technol.* **2026**, *2*, 100019. https://doi.org/10.1016/j.cnt.2026.100019.
35. Steiner, C. *Biochar: Mitigation of Climate Change and Soil Restoration*; Deutsche Gesellschaft für Internationale Zusammenarbeit (GIZ): Eschborn, Germany, 2010. https://d-nb.info/1097402185/34.
36. Radojević, M.; Janković, B.; Stojiljković, D.; et al. Improved TGA-MS measurements for evolved gas analysis (EGA) during pyrolysis process of various biomass feedstocks. Syngas energy balance determination. *Thermochim. Acta* **2021**, *699*, 178912. https://doi.org/10.1016/j.tca.2021.178912.
37. Zhang, S.; Dong, Y.; Qi, G. TG-GC-MS study of pyrolysis characteristics and kinetic analysis during different kinds of biomass. *Int. J. Hydrogen Energy* **2023**, *48*, 11171–11179. https://doi.org/10.1016/j.ijhydene.2022.11.333.
38. Schuepfer, D.B.; Badaczewski, F.; Guerra-Castro, J.M.; et al. Assessing the structural properties of graphitic and non-graphitic carbons by Raman spectroscopy. *Carbon* **2020**, *161*, 359–372. https://doi.org/10.1016/j.carbon.2019.12.094.
39. MP, D.; Misra, M.; Mohanty, A.K. Recent advances on value-added biocarbon preparation by the pyrolysis of renewable and waste biomass, their structure and properties: A move toward an ecofriendly alternative to carbon black. *Environ. Sci. Adv.* **2023**, *2*, 1282–1301. https://doi.org/10.1039/d3va00107e.
40. Dey, S.C.; Lower, L.; Vook, T.; et al. Catalytic graphitization of pyrolysis oil for anode application in lithium-ion batteries. *Green Chem.* **2024**, *26*, 8840–8853. https://doi.org/10.1039/d4gc01647e.
41. Ye, J.; Peng, Q.; Li, D.; et al. Multimodal optimization of synergistic aluminum/nickel catalytic pyrolysis for enhanced hydrogen production from tobacco straw. *Ind. Crops Prod.* **2025**, *237*, 122258. https://doi.org/10.1016/j.indcrop.2025.122258.
42. Gao, N.; Liu, B.; Li, A.; et al. Continuous pyrolysis of pine sawdust at different pyrolysis temperatures and solid residence times. *J. Anal. Appl. Pyrolysis* **2015**, *114*, 155–162. https://doi.org/10.1016/j.jaap.2015.05.011.
43. Desai, H.; Dutta, R.; Panicker, T.F.; et al. Catalytic co-pyrolysis of waste pistachio nutshells and polystyrene: Optimisation of parameters, and catalyst loading on the products yield and composition. *RSC Adv.* **2025**, *15*, 44691–44710. https://doi.org/10.1039/d5ra06092c.
44. Amrullah, A.; Alfiannur, M.; Kusuma, R.B.; et al. Synergistic production of fuel-grade hydrocarbons and carbon-rich biochar from peat soil–plastic waste co-pyrolysis. *Results Eng.* **2026**, *29*, 109154. https://doi.org/10.1016/j.rineng.2026.109154.
45. Yang, Z.; Kumar, A.; Huhnke, R.L.; et al. Pyrolysis of eastern redcedar: Distribution and characteristics of fast and slow pyrolysis products. *Fuel* **2016**, *166*, 157–165. https://doi.org/10.1016/j.fuel.2015.10.101.
46. Wang, M.; Tafti, N.D.; Wang, J.J.; et al. Effect of pyrolysis temperature on Si release of alkali-enhanced Si-rich biochar and plant response. *Biochar* **2021**, *3*, 469–484. https://doi.org/10.1007/s42773-021-00112-3.
47. Zhang, C.; Zhang, Z.; Zhang, L.; et al. Evolution of the functionalities and structures of biochar in pyrolysis of poplar in a wide temperature range. *Bioresour. Technol.* **2020**, *304*, 123002. https://doi.org/10.1016/j.biortech.2020.123002.
48. Zou, X.; Debiagi, P.; Amjed, M.A.; et al. Impact of high-temperature biomass pyrolysis on biochar formation and composition. *J. Anal. Appl. Pyrolysis* **2024**, *179*, 106463. https://doi.org/10.1016/j.jaap.2024.106463.
49. Kabir, G.; Hameed, B.H. Recent progress on catalytic pyrolysis of lignocellulosic biomass to high-grade bio-oil and bio-chemicals. *Renew. Sustain. Energy Rev.* **2017**, *70*, 945–967. https://doi.org/10.1016/j.rser.2016.12.001.
50. Kan, T.; Strezov, V.; Evans, T.; et al. Catalytic pyrolysis of lignocellulosic biomass: A review of variations in process factors and system structure. *Renew. Sustain. Energy Rev.* **2020**, *134*, 110305. https://doi.org/10.1016/j.rser.2020.110305.
51. Dunnigan, L.; Morton, B.J.; Ashman, P.J.; et al. Emission characteristics of a pyrolysis-combustion system for the co-production of biochar and bioenergy from agricultural wastes. *Waste Manag.* **2018**, *77*, 59–66. https://doi.org/10.1016/j.wasman.2018.05.004.
52. Hamidu, I.; Afotey, B.; Kwakye-Awuah, B.; et al. Synthesis of silica and silicon from rice husk feedstock: A review. *Heliyon* **2025**, *11*, e42491. https://doi.org/10.1016/j.heliyon.2025.e42491.
53. Wibowo, W.; Pranolo, S.; Cahyono, R.; et al. Catalytic slow pyrolysis of rice husk pellets with rice husk ash catalyst using macro-TGA: Apparent kinetics and product characterization. *J. Renew. Energy Environ.* **2025**, *12*, 19–32. https://doi.org/10.30501/jree.2025.447645.1870.
54. Chambers, E.; Hassall, M.; Johnson, D.; et al. From bamboo to biochar: A critical review of bamboo pyrolysis conditions and products with a focus on relevance to the developing world. *RSC Sustain.* **2025**, *3*, 2712–2732. https://doi.org/10.1039/d4su00800f.
55. Sarkar, J.K.; Wang, Q. Different pyrolysis process conditions of South Asian waste coconut shell and characterization of gas, bio-char, and bio-oil. *Energies* **2020**, *13*, 1970. https://doi.org/10.3390/en13081970.
56. El-Sayed, S.A. Chemical products yielded from different pyrolysis processes of rice waste residues: A comprehensive review. *Biomass Convers. Biorefinery* **2025**, *15*, 20615–20655. https://doi.org/10.1007/s13399-025-06624-3.
57. Fouladi, S.; Mahmoud, K.A.; Al-Ansari, T.; et al. Techno-economic feasibility of biochar production from local biomass resources in Qatar: A review. *Resour. Conserv. Recycl. Adv.* **2026**, *31*, 200370. https://doi.org/10.1016/j.rcradv.2026.200370.
58. Tang, Y.; Ford, J.; Cockerill, T.T. Environmental and economic assessment of biochar production systems from agricultural residues. *Biochar* **2026**, *8*, 24. https://doi.org/10.1007/s42773-025-00527-2.